Optical-mode hyperconversion in the bad-cavity regime

Jiahua Li* and Ying Wu†

School of Physics, Huazhong University of Science and Technology, Wuhan 430074, People's Republic of China

(Received 2 November 2022; accepted 4 April 2023; published 13 April 2023)

The ability to convert photons between different electromagnetic modes with low intensity has the potential application in future information technologies. Here, we explore optical-mode-conversion characteristics in a bimodal cavity coupled to a pair of two-level atoms instead of a single atom using experimentally realistic parameters. In our scheme, the two cavity modes, involving a vertically (V-) polarized mode and a horizontally (H-) polarized mode, are not directly coupled to each other owing to their orthogonal polarizations and the V-polarized mode is coherently excited by an external weak pump laser. Via analytical calculations and numerical simulations, we find that optical hyperconversion phenomenon from the V-polarized mode to the H-polarized mode can be realized in the bad-cavity regime, which is reminiscent of optical hyperradiance introduced in the previous studies. We also provide an approximate analysis which gains deeper understanding into the fundamental reason behind this behavior. Furthermore, we identify the parameter ranges for generating optical-mode subconversion, superconversion, and hyperconversion. The obtained results will deepen the understanding of mode-conversion micromechanisms in the weak-coupling multiatom cavity architectures.

DOI: 10.1103/PhysRevA.107.043705

I. INTRODUCTION

Cavity quantum electrodynamics (QED) studies light-matter interactions inside microscale and nanoscale structures [1–4], which constitutes an excellent platform to transfer information between light and matter qubits. Also, it has led to many promising applications in areas ranging from one-atom maser and laser [5,6], atom cavity microscopy [7,8], single-photon source [9–11], quantum gate [12,13], to novel quantum information and computation [14–16], etc. As it is known, steering, operating, and converting information in different modes of the electromagnetic field is an important capability of the highly integrated information architecture in the future. A few theoretical and experimental schemes for converting light between different modes, which is called mode conversion, have been proposed based on various cavity QED systems [17–22]. For example, the coherent light generation through spontaneous emission process into an undriven cavity mode under weak excitation of the orthogonally polarized mode has been reported [19]. Incorporating a single quantum emitter into the asymmetric plasmonic cavity has been suggested to realize efficient mode conversion [20]. An optical-mode converter based on cavity QED dark mode in a semiconductor quantum dot coupled to a photonic crystal cavity has been proposed [21].

However, almost all the previous studies about optical-mode conversion have restricted their attention to either the single-emitter cavity QED system, where the light-matter interactions are strongly amplified, or the good-cavity regime, which makes the experimental realization not too easy. One of the goals for cavity QED is to construct interfaces that connect quantum memory stored in atoms to photons that carry information. Putting more atoms into the cavity can improve the connection by increasing the output of the cavity. In 2015, the experiments have uncovered a collective behavior exhibited by two emitters (atoms [23] or ions [24]) isolated in a single cavity, and they measure that the collective light output is greater or less than the sum of single emitters, namely, the so-called superradiant or subradiant [23,24]. Following this, in 2016, interference and dynamics of light from a distance-controlled atom pair in an optical cavity has been explored [25]. Apart from these, recently, in Ref. [26] it has been shown that superradiance can occur in a special networklike architecture for two-level systems interacting with quantized electromagnetic field which is able to significantly improve Rabi frequency between collective spin and cavity modes established by the network topology [27]. On the other hand, in recent years it has been demonstrated that this collective behavior from two individual emitters in optical cavity plays a significant role in hyperradiance [28–31], phonon lasing [32], quantum statistics [33–35], squeezed light [36], and so on. For example, the phase controlled collective behaviors of two atoms in a cavity have been studied [33], showing that the phase difference between the coupling strengths plays an important role in the generation of antibunched or superbunched light field. The squeezed light accompanied by hyperradiance, which is induced by quantum interference in a high-quality optical cavity coupled to two coherently driven two-level qubits with a distance of integer multiple and one-half of wavelengths (i.e., the opposite coupling coefficient to the cavity), has been proposed [36]. Also, much attention has been paid to the so-called bad-cavity regime in which the cavity mode is strongly attenuated with respect to the coupling with the emitters [37–42], i.e., the cavity loss rate is much

*huajia_li@126.com
†yingwu2@126.com

larger than the emitter-cavity coupling. For example, it has been shown in Ref. [39] that the steady-state superradiance can be achieved in the optical frequency domain under the condition that incoherently pumped atoms couple collectively but weakly with a high-Q resonator. Physically, such optical radiation source benefits from the atomic coherence, and can have an extremely narrow linewidth in the mHz range [39]. In Ref. [42] it has been found that there is a dissipative phase transition between the two different phases of steady-state subradiance before the start of steady-state superradiance in a bad cavity laser. This transition arises thanks to the bounded state space of the collective atomic system.

A natural question is thus as follows: What influence does the collective behavior of two separate emitters coupled to a bimodal cavity have on the above-mentioned mode conversion in the bad-cavity regime? Yet, up to now this problem has not received much attention. To address the above concern, with numerical simulations and analytical calculations in the steady state, by utilizing the regime of weak coupling between a pair of two-level atoms and a bimodal optical cavity with orthogonal linear polarizations [i.e., a vertically (V-) polarized mode and a horizontally (H-) polarized mode], we investigate coherent conversion of optical photons from the driven V-polarized mode to the undriven H-polarized mode. The influences of the system parameters on optical-mode conversion are analyzed in detail in the limit of weak pump driving power, finding that optical hyperconversion phenomenon may be attainable under appropriate conditions. Physically, the undriven H-polarized cavity mode is not directly coupled to the input pump laser and the only way it can get light is via the collective emission of both atoms.

In this regard, we perform numerical simulations based on the full quantum master-equation approach beyond the mean-field approximation and give analytical calculations based on the Heisenberg-Langevin equation approach within the mean-field approximation in the weak-driving limit. The analytical results are in excellent agreement with the numerical results. These calculations yield physical insight into the fundamental reason behind optical-mode-hyperconversion behaviors in the bad-cavity regime, and extend hyperradiance effect in a single mode of the electromagnetic field to steering, operating, and converting such a hyperradiance effect in different modes of the electromagnetic field, which is an important ability for future highly integrated photonic information processing. We notice that we work in the bad-cavity regime, which is much easier to achieve, experimentally. Possible applications of the proposed scheme include the control over directionality and tunability of hyperradiance and hyperconversion, achievable with tunable parameters of the system, such as the studies of random lasers [43], as well as the generation of nonclassical fields with hyperradiance and hyperconversion, such as squeezed states and photon antibunching of optical fields [34,36].

Compared with the previous hyperradiance from collective behavior of coherently driven atoms in a single-mode good cavity with strong atom-cavity coupling [28], our scheme is based on a very different operation condition, with the three major advantages that (i) it does not require strong atom-cavity coupling (i.e., it can work in a weak-coupling "bad-cavity" regime), (ii) it extends hyperradiance effect in a single mode of the electromagnetic field to steering, operating, and converting such a hyperradiance effect in different modes of the electromagnetic field, and, (iii) it is more amicable to implement experimentally. In our scheme, we are interested in the intermode (i.e., the V-to-H mode) hyperconversion from collective behavior of two undriven atoms in an orthogonally polarized two-mode cavity and introducing the evaluation parameter is to quantify optical V-to-H mode-conversion ability. Our evaluation parameter is very different from the witness parameter of the work in Ref. [28] as [28] only describes the transmission ability of a singe-mode cavity from two driven atoms rather than the V-to-H mode-conversion ability in an orthogonally polarized two-mode cavity.

The remainder of the article is organized as follows. In Sec. II, we present the physical model of the system under consideration, mainly including the model Hamiltonian, the master equation, and the evaluation parameter. In Sec. III, we give both numerical and analytical methods for estimating the undriven cavity-mode output under steady-state conditions. One is to directly use the quantum master-equation approach (Sec. III A) and the other is to exploit the optical Heisenberg-Langevin equation approach deriving the closed-form solution in the weak-driving limit (Sec. III B). After that, in Sec. V, we analyze and discuss in detail the mode-conversion characteristics from one driven V-polarized mode to the other undriven H-polarized mode in the bad-cavity regime by adjusting the system parameters properly. In Sec. IV, we illustrate the experimental feasibility of our proposed scheme and the selection of relevant system parameters. Finally, the conclusions and outlooks are yielded in Sec. VI. Technical details of the model Hamiltonian derivation are presented in the Appendix.

II. SYSTEM CONSIDERATION AND BASIC EQUATIONS

As shown in Fig. 1, the basic components of our system under consideration are typical of cavity QED architectures. Our cavity QED system consists of an optical cavity where two atoms (qubits) interact with two nearly degenerate cavity modes with orthogonal linear polarizations: a V-polarized cavity mode (resonance frequency ω_V) and a H-polarized cavity mode (resonance frequency ω_H). Here, for concreteness but without loss of generality, we consider a two-mode Fabry-Pérot cavity as our high-finesse optical resonator. Each atom can be considered as a two-level system (transition frequency ω_A) with the ground ($|1\rangle$) and excited ($|2\rangle$) states (see inset). The arrangement of the two atoms trapped inside the cavity is to fix the first atom and scan the second atom along the z axis (i.e., the cavity axis), which results in an interatomic distance Δz corresponding to a relative phase shift ϕ_z. Here, since the distance between the two atoms is assumed to be much larger than the wavelength λ of the cavity photons, the dipole-dipole interaction between them can be safely ignored.

The V-polarized cavity mode is coherently driven along the cavity axis by an external continuous-wave (cw) pump laser $\mathbf{E}_p^{(\mathrm{in})}(t) = \mathbf{e}_V f_p^{(\mathrm{in})} e^{-i\omega_p t}$ with polarization $\mathbf{e}_V$, amplitude $f_p^{(\mathrm{in})}$, and frequency ω_p, through the left-side cavity mirror at an in-coupling rate κ_{le}. On the other hand, the transmitted light through the right-side cavity mirror with an out-coupling rate κ_{re} is collected like in Refs. [19,44]. The starting point for the theoretical model of Fig. 1 is the two-mode Tavis-Cummings

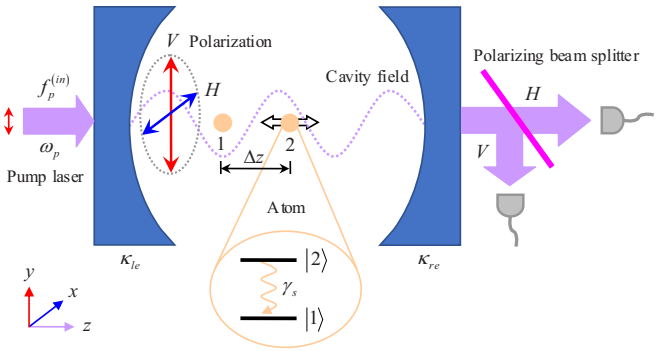

FIG. 1. Schematic of a two-atom cavity QED system used for enhancing photon conversion between different electromagnetic modes. A pair of two-level atoms (resonance frequency ω_A) are coupled to a two-mode cavity with orthogonal linear polarizations involving a vertically (V-) polarized cavity mode (resonance frequency ω_V) and a horizontally (H-) polarized cavity mode (resonance frequency ω_H). Two small tan circles represent the atoms 1 and 2 with the radiative decay rate γ_s. Each atom can be modeled as a two-level system composed of a lower ground state ($|1\rangle$) and an upper excited ($|2\rangle$) state. The configuration to position the two atoms is to fix the atom 1 at an antinode of the cavity field and to vary the atom 2 along the cavity axis (the z direction), thus leading to an interatomic distance Δz which further is associated with a relative phase shift ϕ_z. The two atoms are separated by more than a resonant optical wavelength, so there is no direct (or dipole-dipole) interaction between them. Here, the system is coherently driven by an input vertically polarized pump laser (cavity drive) with a frequency ω_p and an amplitude $f_p^{(\mathrm{in})}$ from the left-side cavity mirror with an in-coupling rate κ_{le} along the cavity axis. The output light (cavity transmission) with the two orthogonal linear polarizations V and H, from the right-side cavity mirror with an out-coupling rate κ_{re}, can be separated through a polarizing beam splitter and then be detected by an avalanche photodiode.

Hamiltonian [45], which, within the dipole and rotating-wave approximations, reads as (see Appendix for details)

$$\begin{aligned}\hat{H}_{\mathrm{tot}} &= \hbar\omega_V \hat{a}_V^\dagger \hat{a}_V + \hbar\omega_H \hat{a}_H^\dagger \hat{a}_H + \hbar\omega_A \hat{\sigma}_1^\dagger \hat{\sigma}_1 + \hbar\omega_A \hat{\sigma}_2^\dagger \hat{\sigma}_2 \\ &\quad + \hbar g_1(\hat{b}\hat{\sigma}_1^\dagger + \hat{b}^\dagger \hat{\sigma}_1) + \hbar g_2\left(\hat{b}\hat{\sigma}_2^\dagger + \hat{b}^\dagger \hat{\sigma}_2\right) \\ &\quad + \hbar\mathcal{E}_p(e^{-i\omega_p t}\hat{a}^\dagger + e^{i\omega_p t}\hat{a}), \end{aligned} \tag{1}$$

where $\hat{a}_V^\dagger$ and $\hat{a}_V$ are the standard creation and annihilation operators of the V- (H-) polarized cavity mode. $\hat{\sigma}_j^\dagger$ and $\hat{\sigma}_j$ ($j = 1, 2$) are the raising and lowering Pauli operators associated with each individual atom with the forms $\hat{\sigma}_j^\dagger = |2\rangle\langle 1|_j$ and $\hat{\sigma}_j = |1\rangle\langle 2|_j$. $\hat{b}^\dagger = \hat{a}_V^\dagger \cos\varphi + \hat{a}_H^\dagger \sin\varphi$ and $\hat{b} = \hat{a}_V \cos\varphi + \hat{a}_H \sin\varphi$ are the cavity photon creation and annihilation operators along the atomic dipole orientation, and φ is the relative angle. The first and second terms in Eq. (1) stand for the energies of the bare two-mode cavity with frequency ω_V (ω_H) for the V- (H-) polarized mode and the third and fourth terms denote the energies of the two bare atoms with frequency ω_A, respectively. The fifth and sixth terms describe the atom-cavity interaction with coupling strength g_j. More specifically, $g_j = g\cos(2\pi z_j/\lambda)$ describes the position-dependent coupling strength between the jth atom and two-mode cavity. As already mentioned above, we assume that the atom 1 is fixed at an antinode of the cavity field, thus we take $g_1 = g$ with $\cos(2\pi z_1/\lambda) = 1$ or $2\pi z_1/\lambda = 2n\pi$ ($n = 0, 1, 2, \ldots$) without loss of generality. However, the position of the atom 2 is varied along the cavity axis with an interatomic distance $\Delta z = z_2 - z_1$ relative to the atom 1 (see Fig. 1). Based on these facts, we have $g_2 = g\cos\phi_z$ where $\phi_z = 2\pi\Delta z/\lambda$ is the relative phase shift induced by the interatomic distance Δz. Two remarks are in order on the implications of the interatomic-distance-induced phase ϕ_z. First, for the case of $\phi_z = n\pi + \pi/2$, the atom 2 is decoupled to the cavity. Second, ϕ_z can be selected (mod 2π) since g_2 is 2π periodic with respect to its phase ϕ_z. In this scenario, the two atoms can be separated by much larger than a resonant optical wavelength λ, such that there is no direct (or dipole-dipole) interaction between them in the above Hamiltonian (1). The last term illustrates the V-polarized pump electromagnetic field injected into the cavity with the frequency ω_p and strength $\mathcal{E}_p$, which is closely related to the amplitude $f_p^{(\mathrm{in})}$ and power P_p of the applied pump laser by the relationships $\mathcal{E}_p = \sqrt{\kappa_{le}} f_p^{(\mathrm{in})} = \sqrt{\kappa_{le} P_p/(\hbar\omega_p)}$.

Moving over to the frame rotating with the pump frequency ω_p, the effective Hamiltonian of the total system in Eq. (1) becomes

$$\begin{aligned}\hat{H}_{\mathrm{eff}} &= \hat{U}^\dagger \hat{H}_{\mathrm{tot}} \hat{U} - i\hat{U}^\dagger \frac{\partial \hat{U}}{\partial t} \\ &= \hbar\Delta_V \hat{a}_V^\dagger \hat{a}_V + \hbar(\Delta_V + \delta_{HV})\hat{a}_H^\dagger \hat{a}_H \\ &\quad + \hbar(\Delta_V + \delta_{AV})\hat{\sigma}_1^\dagger \hat{\sigma}_1 + \hbar(\Delta_V + \delta_{AV})\hat{\sigma}_2^\dagger \hat{\sigma}_2 \\ &\quad + \hbar g(\hat{b}\hat{\sigma}_1^\dagger + \hat{b}^\dagger \hat{\sigma}_1) + \hbar g\cos\phi_z(\hat{b}\hat{\sigma}_2^\dagger + \hat{b}^\dagger \hat{\sigma}_2) \\ &\quad + \hbar\mathcal{E}_p(\hat{a}^\dagger + \hat{a}), \end{aligned} \tag{2}$$

where $\hat{U} = \exp[-i\omega_p(\hat{a}_V^\dagger \hat{a}_V + \hat{a}_H^\dagger \hat{a}_H + \hat{\sigma}_1^\dagger \hat{\sigma}_1 + \hat{\sigma}_2^\dagger \hat{\sigma}_2)t]$ is a unitary transformation operator. $\Delta_V = \omega_V - \omega_p$ is the frequency detuning of the V-polarized cavity mode from the pump laser, $\delta_{HV} = \omega_H - \omega_V$ is the frequency detuning of the H-polarized cavity mode from the V-polarized cavity mode, and $\delta_{AV} = \omega_A - \omega_V$ the frequency detuning of the two-level atoms from the V-polarized cavity mode, respectively.

After taking into account the dissipations of both two-mode cavity and two-level atoms with theirs surrounding environments, the dynamical evolution of the hybrid system is described by the following Lindblad master equation under the Born-Markov approximation [46–48]:

$$\begin{aligned}\frac{d\hat{\rho}}{dt} &= -i[\hat{H}_{\mathrm{eff}}, \hat{\rho}] + \kappa\mathcal{D}(\hat{a}_V)\hat{\rho} + \kappa\mathcal{D}(\hat{a}_H)\hat{\rho} + \gamma_s\mathcal{D}(\hat{\sigma}_1)\hat{\rho} \\ &\quad + \gamma_s\mathcal{D}(\hat{\sigma}_2)\hat{\rho}, \end{aligned} \tag{3}$$

where $\mathcal{D}(\hat{\mathcal{O}})\hat{\rho} = \hat{\mathcal{O}}\hat{\rho}\hat{\mathcal{O}}^\dagger - 1/2\hat{\rho}\hat{\mathcal{O}}^\dagger\hat{\mathcal{O}} - 1/2\hat{\mathcal{O}}^\dagger\hat{\mathcal{O}}\hat{\rho}$ is a general Lindbald superoperator form for the collapse operator $\hat{\mathcal{O}} \in \{\hat{a}_V, \hat{a}_H, \hat{\sigma}_1, \hat{\sigma}_2\}$, accounting for the losses to the environments. Notice that the definition of γ_s and κ in the dissipator superoperator terms of Eq. (3) differs by a factor of 2 compared to that in Refs. [25,49]. Above, the thermal photon numbers have been neglected in the low-temperature limit because of the extra high frequencies of the V and H cavity modes. $\hat{\rho}$ is the density matrix operator of the total atom-cavity coupled system and $\hat{H}_{\mathrm{eff}}$ is directly given by Eq. (2). $\kappa = \kappa_i + \kappa_{le} + \kappa_{re}$ is the total loss rate of the cavity mode,

where κ_i is the intrinsic loss rate of the cavity, and κ_{le} (κ_{re}) is the external loss rate of the left (right) cavity mirror. The former is due to undesirable absorption and scattering inside the cavity, whereas the latter is owing to the extraction of cavity photons to the desired external mode via transmission of the mirror. Last but not least, the external loss can be experimentally controlled by tuning or designing the transmissivity of the output coupler, for example, the cavity mirror. γ_s is the decay rate of the two-level atom.

According to the input-output formalism [47,48], the operator $\hat{f}_H$ of interest to us here, which describes the transmission field of the undriven H-polarized cavity mode through the right-side mirror (see Fig. 1), can be written as follows:

$$\hat{f}_H = -i\sqrt{\kappa_{re}}\hat{a}_H, \tag{4}$$

which is directly proportional to the intracavity field $\hat{a}_H$ of the H polarization. The output photon flux $\langle \hat{f}_H^\dagger \hat{f}_H \rangle$ is proportional to the average number of cavity photons $\langle \hat{a}_H^\dagger \hat{a}_H \rangle$. As final remark, here we point out that, in fact, the multimode vacuum inputs of the cavity on the right cavity mirror can exist, even a vacuum field reflecting off of the cavity in Fig. 1. The corresponding input noise operators due to the vacuum field should be added to the right-hand side of Eq. (4) in order to preserve the bosonic commutation relation. These input noise operators and their normally ordered moments have zero mean values as was shown already in standard textbooks: for quantum optics, see, e.g., Ref. [37]. Therefore, the later calculation results will not be affected. Also, the related terms are not included in Eq. (4) explicitly.

Correspondingly, making use of Eq. (4), the normalized intensity transmission T_j ($j = 1, 2$), namely, the ratio of the number of the resulting output photons per unit time in the H polarization to the input photons in the pump laser, can be given by the formula

$$T_j = \frac{\langle \hat{f}_H^\dagger \hat{f}_H \rangle_j}{\left| f_p^{(\mathrm{in})} \right|^2} = \frac{\mathrm{Tr}(\hat{\rho} \hat{f}_H^\dagger \hat{f}_H)_j}{\left| f_p^{(\mathrm{in})} \right|^2}, \tag{5}$$

where $\langle \cdot \rangle$ denotes the quantum expectation value and Tr the trace. For convenience of comparison below, we have introduced the subscript j. T_2 means the average intensity transmission for two atoms ($j = 2$) in the cavity, while T_1 corresponds to the average intensity transmission for only one atom ($j = 1$) in the cavity. It is worth pointing out that T_i also can be regarded as the overall photon mode-conversion efficiency because it is the ratio of the output photon flux $\langle \hat{f}_H^\dagger \hat{f}_H \rangle_j$ for the undriven H-polarized mode over the input photon flux $|f_p^{(\mathrm{in})}|^2$ for the driven V-polarized mode.

On the other hand, the ability and behavior of optical-mode conversion from the V-polarized to H-polarized mode in the two-atom cavity QED system can be quantified by the following evaluation parameter W, defined as

$$W = T_2 - 2T_1, \tag{6}$$

where T_1 is a reference value of a single atom positioned at an antinode of the cavity field and the factor 2 appearing in front of T_1 is introduced in order to compare the mode-conversion efficiency for the coupled two-atom system with that for the system of two uncorrelated atoms, which is analogous to that introduced in Ref. [50]. T_1 and T_2 are given by Eq. (5). Several remarks are in order on the implications of Eq. (6).

First of all, $W = 0$, i.e., $T_2 = 2T_1$, represents the fact that optical-mode conversion for the two-atom cavity system is simply the sum of that for two independent atoms in the cavity, namely, an uncorrelated conversion for two atoms.

Second, $W < 0$, i.e., $T_2 < 2T_1$, indicates that the mode conversion is suppressed for the two-atom cavity system, which is called mode subconversion, analogous to subradiance [51].

Third, $W > 0$, i.e., $T_2 > 2T_1$, reveals an enhanced mode conversion. Interestingly, $W = 2T_1$, i.e., $T_2 = 4T_1$, implies that the mode conversion scales with the square of the number of atoms in the cavity, which is reminiscent of superradiance [51], therefore referred to as mode superconversion. In particular, when $W > 2T_1$, i.e., $T_2 > 4T_1$, this implies that the mode conversion is significantly enhanced, which is defined as the mode hyperconversion.

To sum up, when the two atoms in a two-mode cavity, where the V-polarized mode is coherently driven, cooperatively radiate at smaller, just twice times higher, or more than twice times higher optical power into another undriven H-polarized cavity mode than the two independent atoms, in turn we call it subconversion, superconversion, or hyperconversion, namely, the so-called evaluation parameter. So, it quantifies optical V-to-H mode-conversion ability in an orthogonally polarized two-mode cavity.

III. CALCULATIONS OF INTENSITY TRANSMISSION AND EVALUATION PARAMETER

A. Numerical solution using Born-Markov quantum master-equation approach

In order to find the steady state of the system $\hat{\rho}(t \to \infty)$, we can numerically solve the master Eq. (3) with the left-hand side set to zero (i.e., $d\hat{\rho}/dt = 0$), from which we can calculate the average value of every observable of the system using the relation $\langle \hat{O} \rangle = \mathrm{Tr}(\hat{\rho}\hat{O})$. Of interest to us here are the intensity transmission T_j and the evaluation parameter W. For this purpose, we truncate the Hilbert space of two cavity modes at photon numbers sufficiently large to ensure full convergence, which depends on the pump laser strength $\mathcal{E}_p$ in Eq. (2). Here, the considered Hilbert space is expanded by the electronic states of the two two-level atoms and the Fock states of the two cavity modes. The main aim is to check the accuracy of the analytical solution presented below.

B. Analytical solution using Heisenberg-Langevin equation approach in the weak-driving limit

The intensity transmission in Eq. (5) and the evaluation parameter W in Eq. (6) can also be analytically calculated in the weak-pumping limit, that provides further physical insight into the numerical results. To this end, we focus on the case of a rather small $\mathcal{E}_p$ in the following.

By multiplying the master equation (3) with the given operator $\hat{O} \in \{\hat{a}_V, \hat{a}_H, \hat{\sigma}_1, \hat{\sigma}_2\}$, performing the trace operation, and applying the cyclic permutation of the trace, it is straightforward to attain the Heisenberg-Langevin equations of motion

for the mean values of the operators $\langle\hat{a}_V\rangle$, $\langle\hat{a}_H\rangle$, $\langle\hat{\sigma}_1\rangle$, and $\langle\hat{\sigma}_2\rangle$:

$$\frac{d\langle\hat{a}_V\rangle}{dt} = -i(\Delta_V - i\kappa/2)\langle\hat{a}_V\rangle - ig\cos\varphi\langle\hat{\sigma}_1\rangle - ig\cos\phi_z\cos\varphi\langle\hat{\sigma}_2\rangle - i\mathcal{E}_p, \tag{7}$$

$$\frac{d\langle\hat{a}_H\rangle}{dt} = -i(\Delta_V + \delta_{HV} - i\kappa/2)\langle\hat{a}_H\rangle - ig\sin\varphi\langle\hat{\sigma}_1\rangle - ig\cos\phi_z\sin\varphi\langle\hat{\sigma}_2\rangle, \tag{8}$$

$$\frac{d\langle\hat{\sigma}_1\rangle}{dt} = -i(\Delta_V + \delta_{AV} - i\gamma_s/2)\langle\hat{\sigma}_1\rangle + ig\cos\varphi\langle\hat{a}_V\hat{\sigma}_{z1}\rangle + ig\sin\varphi\langle\hat{a}_H\hat{\sigma}_{z1}\rangle, \tag{9}$$

$$\frac{d\langle\hat{\sigma}_2\rangle}{dt} = -i(\Delta_V + \delta_{AV} - i\gamma_s/2)\langle\hat{\sigma}_2\rangle + ig\cos\phi_z\cos\varphi\langle\hat{a}_V\hat{\sigma}_{z2}\rangle + ig\cos\phi_z\sin\varphi\langle\hat{a}_H\hat{\sigma}_{z2}\rangle, \tag{10}$$

where $\hat{\sigma}_{zj} = \hat{\sigma}_j^\dagger\hat{\sigma}_j - \hat{\sigma}_j\hat{\sigma}_j^\dagger$ is the population-difference operator of atom j ($j = 1, 2$) between the ground state $|1\rangle_j$ and the excited state $|2\rangle_j$ with $\hat{\sigma}_j^\dagger = |2\rangle\langle 1|_j$ and $\hat{\sigma}_j = |1\rangle\langle 2|_j$, namely, $\hat{\sigma}_{zj} = |2\rangle\langle 2|_j - |1\rangle\langle 1|_j$. In the limit of low-pump excitation mentioned above, the two-level atomic system is approximately in its ground state, so we can take $\hat{\sigma}_{zj} \simeq -1$. As can be seen, the operators $\hat{\sigma}$ and $\hat{\sigma}^\dagger$ satisfy the bosonic commutation relation, i.e., $[\hat{\sigma}_j, \hat{\sigma}_j^\dagger] = -\hat{\sigma}_{zj} \simeq 1$. In this situation, the two-level atomic system can be treated as a good model for a harmonic oscillator. Therefore, we can set $\langle\hat{a}_V\hat{\sigma}_{zj}\rangle \simeq -\langle\hat{a}_V\rangle$ and $\langle\hat{a}_H\hat{\sigma}_{zj}\rangle \simeq -\langle\hat{a}_H\rangle$ in Eqs. (9) and (10). Under the steady-state condition, utilizing the above approximation, Eqs. (7)–(10) can then be simplified into the following algebraic forms:

$$f_1\langle\hat{a}_V\rangle = -g\cos\varphi\langle\hat{\sigma}_1\rangle - g\cos\phi_z\cos\varphi\langle\hat{\sigma}_2\rangle - \mathcal{E}_p, \tag{11}$$

$$f_2\langle\hat{a}_H\rangle = -g\sin\varphi\langle\hat{\sigma}_1\rangle - g\cos\phi_z\sin\varphi\langle\hat{\sigma}_2\rangle, \tag{12}$$

$$f_3\langle\hat{\sigma}_1\rangle = -g\cos\varphi\langle\hat{a}_V\rangle - g\sin\varphi\langle\hat{a}_H\rangle, \tag{13}$$

$$f_3\langle\hat{\sigma}_2\rangle = -g\cos\phi_z\cos\varphi\langle\hat{a}_V\rangle - g\cos\phi_z\sin\varphi\langle\hat{a}_H\rangle, \tag{14}$$

where we have defined $f_1 = \Delta_V - i\kappa/2$, $f_2 = \Delta_V + \delta_{HV} - i\kappa/2$, and $f_3 = \Delta_V + \delta_{AV} - i\gamma_s/2$, respectively.

After some tedious but straightforward calculations, the steady-state solution of Eqs. (11)–(14) about $\langle\hat{a}_H\rangle$ can be found as

$$\frac{\langle\hat{a}_H\rangle}{f_p^{(\mathrm{in})}} = \frac{2f_3\sqrt{\kappa_{le}}g^2(1+\cos^2\phi_z)\sin 2\varphi}{g^4(1+\cos^2\phi_z)^2\sin^2 2\varphi - 4(f_1f_3 - g^2\cos^2\varphi - g^2\cos^2\varphi\,\cos^2\phi_z)(f_2f_3 - g^2\sin^2\varphi - g^2\sin^2\varphi\,\cos^2\phi_z)}, \tag{15}$$

from which we subsequently can acquire the normalized intensity transmission $T_2 = \kappa_{re}|\langle\hat{a}_H\rangle/f_p^{(\mathrm{in})}|^2$ for the two-atom case. The closed-form solution (15) is the starting point of the analytical discussion of optical-mode conversion in the following. Here it is emphasized that, if $\phi_z = \pi/2$, the expression of T_2 reduces to that of T_1 for the one-atom case. Additionally, T_2 is of π periodicity with respect to ϕ_z and is of $\pi/2$ periodicity with respect to φ.

IV. RESULTS AND DISCUSSION ABOUT EFFICIENT MODE CONVERSION

In what follows, we will start by looking at optical-mode-conversion characteristics in a bimodal optical cavity mediated by the two atoms for experimentally realistic parameters. Figure 2(a) shows the normalized intensity transmissions of the undriven H-polarized cavity mode: T_2 for the two-atom case and T_1 for the one-atom case, as a function of the frequency detuning Δ_V/γ_s. As a matter of fact, T_2 and T_1 also represent the conversion efficiency form the driven V-polarized cavity mode to the undriven H-polarized cavity mode. As can be seen from Fig. 2(a), T_2 reaches its maximal value of 0.032 at $\Delta_V/\gamma_s = -0.02$, beyond which it rapidly decreases to reach a vanishingly small value. A similar curve is found for T_1, but the maximal value of T_1 is only 0.012. From this analysis it is clear that $T_2 > 2T_1$ exists, and the enhanced mode conversion can be achieved. As a check, we compare the numerical results from the master equation (3) and the analytical estimates from the formulas (15), finding that they are consistent.

Physically, the driven V mode excites the $|1\rangle \leftrightarrow |2\rangle$ transition in the atoms through the pump laser, and the cw pump driving of this mode introduces the energy into the system. Some of these energies are transferred to the undriven H mode by the excitation and decay of both atoms. The difference in peak height between both scenarios is thanks to an enhanced collective emission induced by the two atoms in the cavity [23–25]. On the other hand, it should be pointed out that a nonzero small value of Δ_V corresponding to the appearance of the maximal intensity transmission in Fig. 2(a) is due to the fact that we consider the slight splitting of $\delta_{HV}/\gamma_s = 0.08$ between the V and H modes in the calculation as a result of fabrication imperfections in a realistic system [20,44]. When setting $\delta_{HV} = 0$, as expected the maximal intensity transmission occurs at $\Delta_V = 0$ (not shown here). Figure 2(b) depicts the evaluation parameter W of optical-mode-conversion ability together with $2T_1$ as a function of the detuning Δ_V/γ_s. The main purpose is to assess the quality of the mode conversion of the two-atom system, through performing a reference simulation of a single atom located at the antinode of the cavity fields. From these plots, we can see that $W > 0$ can be well obtained in the approximate range of $-1 < \Delta_V/\gamma_s < 1$. At $\Delta_V/\gamma_s = 0.5$ and $\Delta_V/\gamma_s = 1$ as shown in the inset, we observe $W = 2T_1$ (i.e., $T_2 = 4T_1$) as a clear sign of

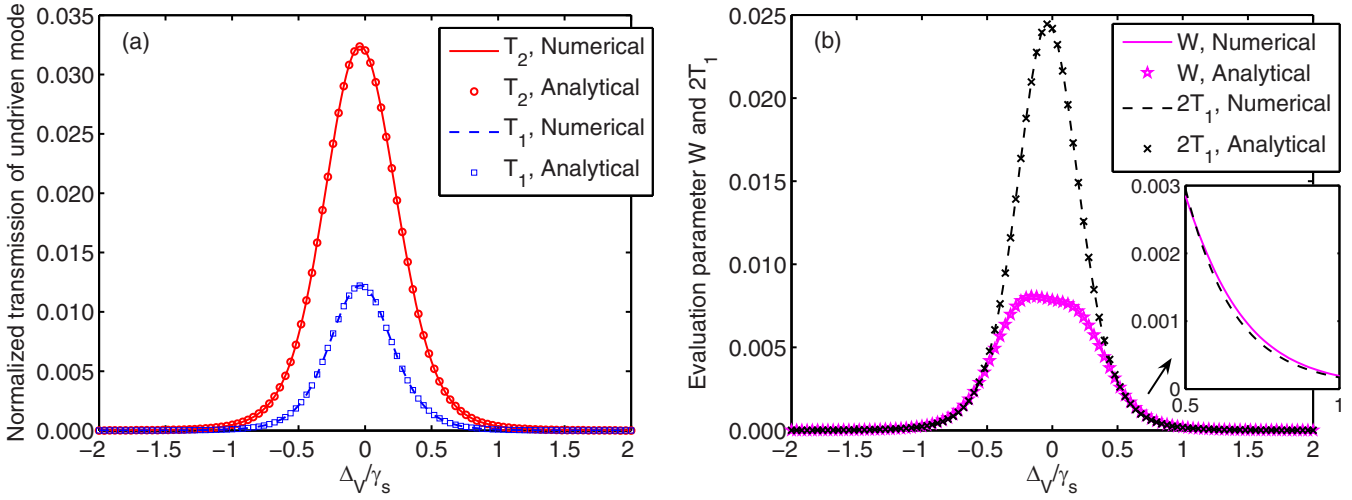

FIG. 2. (a) Intensity transmissions T_2 of the undriven H-polarized cavity mode in the two-atom case as a function of the detuning Δ_V/γ_s, and T_1 in the one-atom case. Here, the transmission is normalized to the intensity of the input pump laser driving the V-polarized cavity mode, which also describes the conversion efficiency from the driven V-polarized mode to the undriven H-polarized mode. (b) Evaluation parameter $W \equiv T_2 - 2T_1$, showing the conversion degree of the V-to-H mode with two atoms in comparison to one atom, as a function of the detuning Δ_V/γ_s, and also twice the intensity transmission $2T_1$ for the one-atom case for comparison. The red solid and blue dashed curves in (a) and the magenta solid and black dashed curves in (b) are the numerical simulations obtained using Eq. (3), while the red circle and blue square markers in (a) and the magenta star and black cross markers in (b) are the analytical results calculated from Eq. (15). The inset in (b) emphasizes the region of $\Delta_V/\gamma_s \in [0.5, 1]$ where both $W \geqslant 2T_1$ and $T_2 > 0$ in the main panels. The system parameters for all the results are $g = 0.25\gamma_s$, $\kappa_{le} = \kappa_{re} = 0.4\gamma_s$, $\kappa_i = 0.03\gamma_s$, $\delta_{HV} = 0.08\gamma_s$, $\delta_{AV} = 0$, $\phi_z = 0$, $\varphi = \pi/4$, and $\mathcal{E}_p = 0.01\gamma_s$.

optical-mode superconversion. In particular, in the ranges of $0.5 < \Delta_V/\gamma_s < 1$ and $-1 < \Delta_V/\gamma_s < -0.5$, we find $W > 2T_1$ (i.e., $T_2 > 4T_1$), manifesting optical-mode hyperconversion. Notice that, for a significantly large detuning, for example, $\Delta_V/\gamma_s = 1.5$, both T_2 and T_1 are equal to zero, which should be excluded from the above obtainable conclusions.

To gain a more quantitative insight and simplify the analysis, as above, we now focus on some parameter values, such as $\Delta_V = 0$, $\delta_{AV} = 0$, $\varphi = \pi/4$, and $\delta_{HV} \to 0$. In this scenario, based on Eq. (15), the normalized intensity transmission T_2 can be rewritten as

$$T_2 = \left[\frac{g^2\sqrt{\kappa_{le}}\sqrt{\kappa_{re}}}{g^2\kappa + \frac{\kappa^2\gamma_s}{4(1+\cos^2\phi_z)}}\right]^2, \tag{16}$$

from which we can clearly see that T_2 reaches a maximum at $\phi_z = 0$ (in-phase coupling of two atoms) or π (out-of-phase coupling of two atoms), whereas it has a minimum at $\phi_z = \pi/2$ (decoupling of one atom). For example, provided the aforementioned criterion $W = 0$, under the given g, κ, and γ_s, from Eq. (16) we can derive the following condition about ϕ_z:

$$\phi_z = \arccos\left[\frac{\sqrt{2}}{1-(\sqrt{2}-1)C} - 1\right] \tag{17}$$

or

$$\phi_z = \pi - \arccos\left[\frac{\sqrt{2}}{1-(\sqrt{2}-1)C} - 1\right], \tag{18}$$

where $C = 4g^2/(\kappa\gamma_s)$ is the cooperativity parameter. If ϕ_z is located in the range of $\arccos[\frac{\sqrt{2}}{1-(\sqrt{2}-1)C} - 1] < \phi_z < \pi - \arccos[\frac{\sqrt{2}}{1-(\sqrt{2}-1)C} - 1]$, then we can get $W < 0$. Otherwise, beyond this range in a periodicity of π, we have $W > 0$. For the intensity transmission corresponding to the situation of an off-resonant pump laser ($\Delta_V \neq 0$), the tedious expressions offer no clear physical insight, thus they are not given here.

In Figs. 3(a) and 3(b), we show how the intensity transmission T_2 (or T_1) of the undriven H-polarized cavity mode and the evaluation parameter W changes as a function of the relative phase ϕ_z induced by the interatomic distance Δz in Fig. 1. Specifically, for the case of a pair of atoms in the cavity as shown by the red solid line in Fig. 3(a), the intensity transmission T_2 exhibits a clear π-periodic change with respect to ϕ_z. Moreover, from Fig. 3(a), we can find that T_2 reaches a maximum value when $\phi_z = 0$ or π. However, T_2 reaches a minimum value when $\phi_z = \pi/2$ because the second atom just is decoupled from the cavity fields. These are in agreement with the analytic prediction of Eq. (16). As mentioned before, in the atomic position with $\phi_z = \pi/2$, the system is equivalent to that for the scenario of a single atom in the cavity, as a result T_2 and T_1 intersect at one point with an equal value $T_2 = T_1$. Apart from that, we observe the following: T_2 decreases with the increasing of ϕ_z from 0 to $\pi/2$. Instead, T_2 increases with increasing ϕ_z from $\pi/2$ to π. Shown by the blue dashed line in Fig. 3(a) is T_1 versus ϕ_z for the case of only a single atom in the cavity as a comparison. Quite evidently, the phase factor ϕ_z during the atom-field coupling can not appear at all, therefore, the intensity transmission T_1 is a straight line and is irrelevant to ϕ_z.

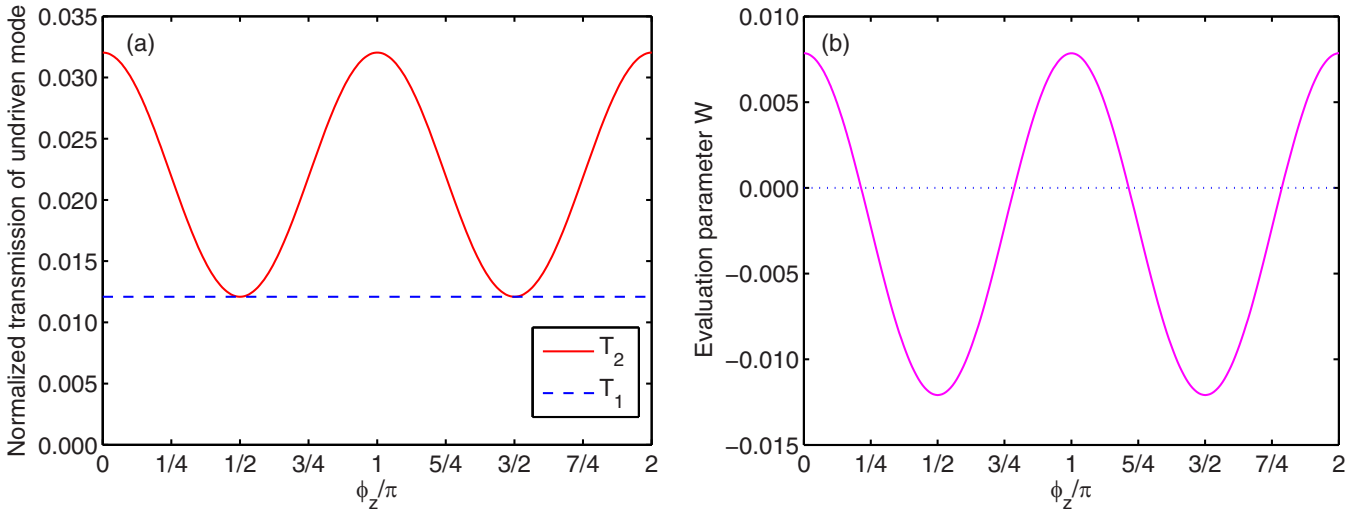

FIG. 3. (a) Normalized intensity transmissions T_2 of the undriven H-polarized cavity mode in the two-atom case as a function of the interatomic-distance-induced phase ϕ_z/π, and T_1 in the one-atom case. (b) Evaluation parameter W of optical-mode-conversion ability as a function of the interatomic-distance-induced phase ϕ_z/π. Here, the system parameters are $g = 0.25\gamma_s$, $\kappa_{le} = \kappa_{re} = 0.4\gamma_s$, $\kappa_i = 0.03\gamma_s$, $\delta_{HV} = 0.08\gamma_s$, $\delta_{AV} = 0$, $\Delta_V = 0$, $\varphi = \pi/4$, and $\mathcal{E}_p = 0.01\gamma_s$.

As shown in Fig. 3(b), the evaluation parameter W of optical-mode-conversion ability exhibits a strong phase-dependent effect. First, W decreases with increasing ϕ_z from 0 to $\pi/2$. Beyond $\phi_z = \pi/2$, a further increase in ϕ_z increases W in the π periodicity. Aside from this, it can be seen that $W = 0$ at $\phi_z \simeq \pi/5$ and $4\pi/5$. According to Eqs. (17) and (18), for the given parameters in Fig. 3(b), we obtain $\phi_z \simeq \pi/5$ corresponding to $W = 0$. The numerical results confirm our analytical results. In the ranges of $0 < \phi_z < \pi/5$ and $4\pi/5 < \phi_z < \pi$, we have the evaluation parameter $W > 0$, corresponding to the enhanced mode conversion in the two-atom system. However, in the range of $\pi/5 < \phi_z < 4\pi/5$, we have $W < 0$, reflecting optical-mode subconversion. In light of the above analysis, we find that the V-to-H-mode conversion displays these features that are not expected in a simple picture of two uncorrelated atoms emitting into the H-polarized cavity mode.

In order to further show explicitly the dependency of the mode conversion on the detuning Δ_V and the phase ϕ_z, we plot, in color, the two-dimensional (2D) density distribution of the normalized intensity transmissions T_2 [Fig. 3(a)], the evaluation parameter W [Fig. 3(b)], and another evaluation parameter $W - 2T_1$ [Fig. 3(c)] in Figs. 4(a)–4(c), enabling direct comparison between the three data sets. Looking closer, we see that the regions of all $T_2 > 0$, $W > 0$, and $W - 2T_1 > 0$ can be generated by appropriately choosing Δ_V and ϕ_z. This suggests the possibility of optical-mode hyperconversion, reminiscent of driven-atom hyperradiance [28]. In Figs. 5(a) and 5(b) the dependencies of the intensity transmission T_2 (or T_1) of the undriven H-polarized cavity mode and the evaluation parameter W are checked against the atom-cavity coupling strength g (note the logarithm scale of the horizontal axis). As follows from Fig. 5(a), the intensity transmission T_2 is seen to monotonically increase with increasing g and then saturates at higher g shown, e.g., $g \sim 10\gamma_s$. Analogously, as g increases, so does the intensity transmission T_1, and it ultimately reaches a saturated state for larger g. The difference between the one- and two-atom coupling situations is that T_2 is larger than T_1 in an intermediate regime of g.

Physically, this behavior can be understood by introducing the mentioned-above cooperativity parameter $C = 4g^2/(\kappa\gamma_s)$. For the case of a symmetric cavity $\kappa_{le} = \kappa_{re} = \eta\kappa$ and $\eta = \kappa_{le}/\kappa = 40/83$ given in Fig. 5, we can reexpress Eq. (16) in terms of C as

$$T_2 = \left(\frac{\eta C}{C + \frac{1}{1+\cos^2\phi_z}}\right)^2, \tag{19}$$

from which, we can know that (i) $C \ll 1$, T_2 approaches 0; and (ii) $C \gg 1$, T_2 approaches η^2, i.e., $T_2 \simeq 0.23$ in Fig. 5. For the one-atom case, $\phi_z = \pi/2$ directly leads to $T_1 = (\frac{\eta C}{C+1})^2$. So, between (i) and (ii), we have the relation $T_2 > T_1$.

Further, when $\phi_z = 0$ or π for the two-atom case and $\phi_z = \pi/2$ for the one-atom case, the normalized intensity transmissions T_2 and T_1 can be explicitly expressed as

$$T_2 = \left(\frac{g^2\sqrt{\kappa_{le}}\sqrt{\kappa_{re}}}{g^2\kappa + \kappa^2\gamma_s/8}\right)^2 \quad \text{for two atoms,} \tag{20}$$

$$T_1 = \left(\frac{g^2\sqrt{\kappa_{le}}\sqrt{\kappa_{re}}}{g^2\kappa + \kappa^2\gamma_s/4}\right)^2 \quad \text{for one atom.} \tag{21}$$

From Eqs. (20) and (21), one can easily see that the appearance of an uncorrelated conversion $W = 0$ requires the following condition for the denominators in the parentheses: $g^2\kappa + \kappa^2\gamma_s/4 = \sqrt{2}(g^2\kappa + \kappa^2\gamma_s/8)$, because the numerators are the same. After some calculations, we obtain a more compact relation

$$g = \sqrt{\sqrt{2}\kappa\gamma_s/8}, \tag{22}$$

for this critical point $W = 0$. Similarly, when the condition $g > \sqrt{\sqrt{2}\kappa\gamma_s/8}$ holds, optical-mode subconversion $W < 0$ emerges. By contrast, $g < \sqrt{\sqrt{2}\kappa\gamma_s/8}$ results in $W > 0$. With

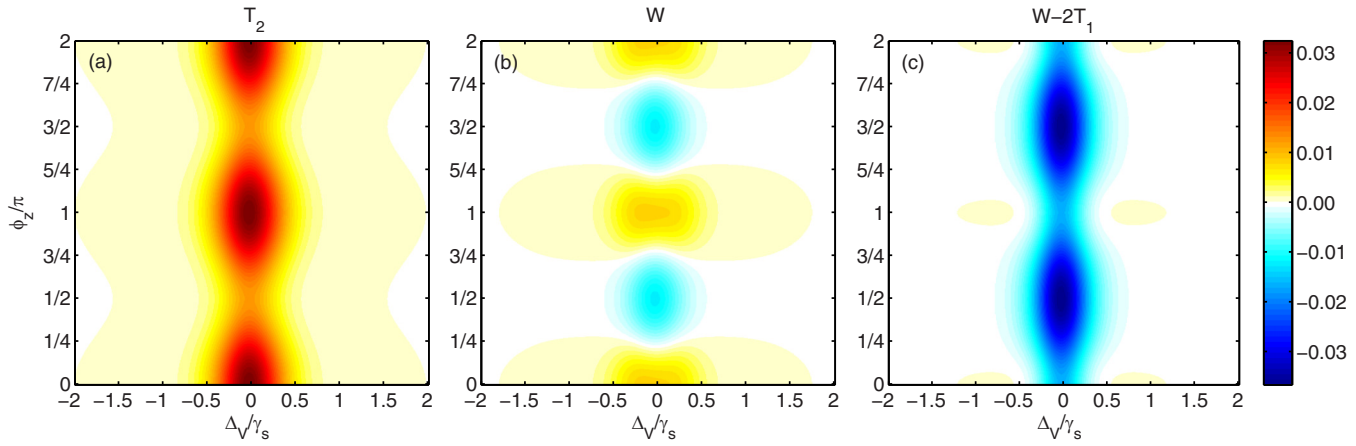

FIG. 4. Contour plots of (a) the normalized intensity transmissions T_2 of the undriven H-polarized cavity mode in the two-atom case, (b) evaluation parameter W of optical-mode-conversion ability, and (c) another evaluation parameter $W - 2T_1$ versus the detuning Δ_V/γ_s and the interatomic-distance-induced phase ϕ_z/π. (a)–(c) Share the same color bar. The system parameters are $g = 0.25\gamma_s$, $\kappa_{le} = \kappa_{re} = 0.4\gamma_s$, $\kappa_i = 0.03\gamma_s$, $\delta_{HV} = 0.08\gamma_s$, $\delta_{AV} = 0$, $\varphi = \pi/4$, and $\mathcal{E}_p = 0.01\gamma_s$.

these parameters at hand (see Fig. 5), we have $g/\gamma_s \simeq 0.383$ at $W = 0$.

As shown in Fig. 5(b), first the evaluation parameter W from a zero value grows slowly with the atom-cavity coupling strength g and reaches a positive maximum around $g/\gamma_s = 0.28$. With the increase of g above the optimal value $g/\gamma_s = 0.28$, W then starts to decrease rapidly. In the meantime, the demarcation point $W = 0$ arises at $g/\gamma_s \simeq 0.383$ in excellent agreement with the analytical formulas (22). And, in this regard, W takes negative values when $g/\gamma_s > 0.383$ (see inset).

To gain further insight, we simultaneously consider the effect of detuning the pump laser from the driven V-polarized cavity mode and scanning the atom-cavity coupling strength. Figures 6(a)–6(c) show the evolution of T_2, W, and $W - 2T_1$ as a function of Δ_V and g, which exhibits a pronounced mode hyperconversion regime. It shows that detuning the driving pump laser is preferred to obtain optical-mode hyperconversion. In Figs. 7(a)–7(c) we plot T_2, W, and $W - 2T_1$ as a function of ϕ_z and g, considering the on-resonance case $\Delta_V = 0$. It reveals that, regardless of what both ϕ_z and g are set to, there is no mode hyperconversion because of $W - 2T_1 \leqslant 0$. As a further remark, we note that the values of $W > 0$ appearing in Fig. 7(b) are indicative of mode-conversion enhancement, to a certain extent. On the contrary, in a detuned case, i.e., for $\Delta_V/\gamma_s = 1$ in Figs. 8(a)–8(c), the other

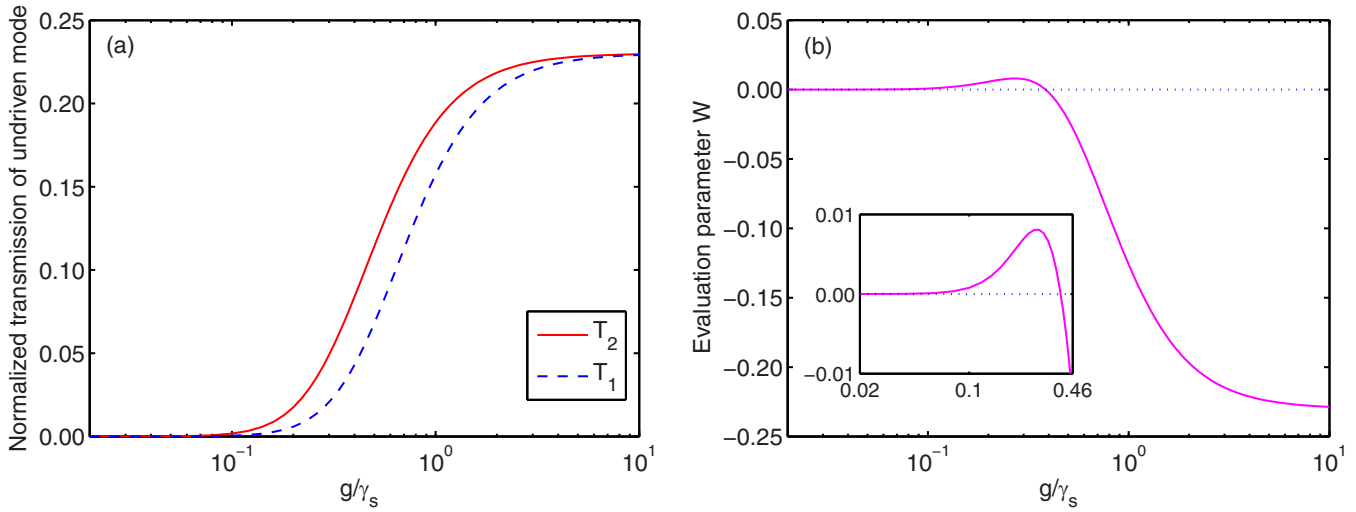

FIG. 5. (a) Normalized intensity transmissions T_2 of the undriven H-polarized cavity mode in the two-atom case as a function of the atom-cavity coupling strength g/γ_s, and T_1 in the one-atom case. (b) Evaluation parameter W of optical-mode-conversion ability as a function of the atom-cavity coupling strength g/γ_s. The inset of (b) shows the zoomed-in region of $W > 0$ for clarity. In all panels, the horizontal axis is plotted in logarithmic scale. Other unspecified system parameters are $\kappa_{le} = \kappa_{re} = 0.4\gamma_s$, $\kappa_i = 0.03\gamma_s$, $\delta_{HV} = 0.08\gamma_s$, $\delta_{AV} = 0$, $\Delta_V = 0$, $\phi_z = 0$, $\varphi = \pi/4$, and $\mathcal{E}_p = 0.01\gamma_s$.

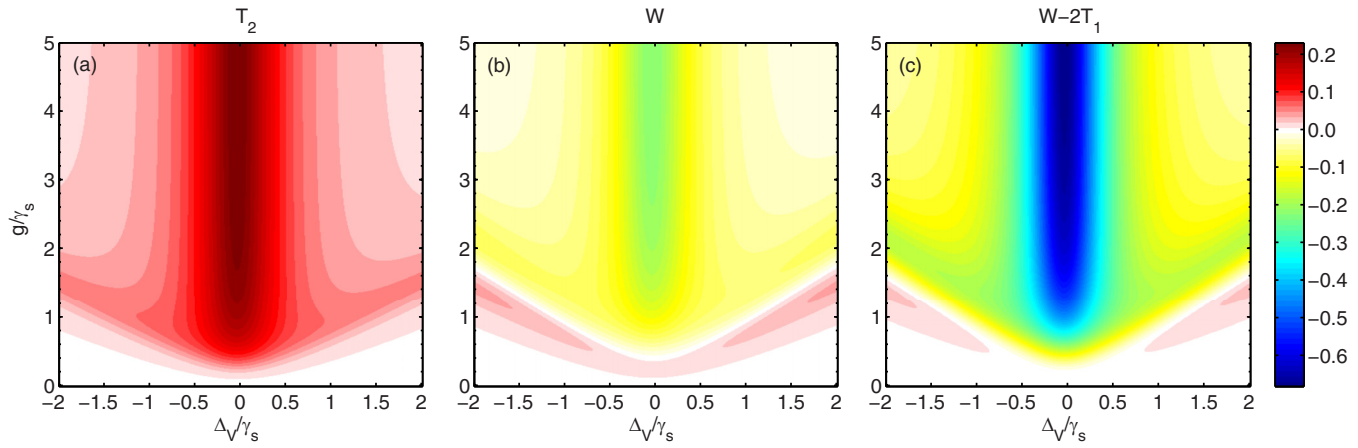

FIG. 6. Contour plots of (a) the normalized intensity transmissions T_2 of the undriven H-polarized cavity mode in the two-atom case, (b) evaluation parameter W of optical-mode-conversion ability, and (c) another evaluation parameter $W - 2T_1$ versus the detuning Δ_V/γ_s and the atom-cavity coupling strength g/γ_s. The system parameters are $\kappa_{le} = \kappa_{re} = 0.4\gamma_s$, $\kappa_i = 0.03\gamma_s$, $\delta_{HV} = 0.08\gamma_s$, $\delta_{AV} = 0$, $\phi_z = 0$, $\varphi = \pi/4$, and $\mathcal{E}_p = 0.01\gamma_s$.

parameters remaining the same as Figs. 7(a)–7(c), one observes that optical-mode hyperconversion $W - 2T_1 > 0$ can be obtained. Once again, it turns out that detuning the V-polarized cavity mode and pump laser resonances enables the generation of optical-mode hyperconversion.

Following the analogy of Eqs. (4) and (5) in Sec. II, for the driven V-polarized cavity mode, we define the normalized intensity transmission denoted by I_2 for two atoms and I_1 for only one atom when replacing the subscript H with V in Eqs. (4) and (5). We begin by studying a normalized intensity transmission for the driven V-polarized cavity mode as the one for the undriven H-polarized cavity mode. The result is shown in Fig. 9, finding that I_2 in the two-atom case is smaller than I_1 in the one-atom case, which is opposite to that in Fig. 2(a). This is because of optical-mode-conversion enhancement under the two-atom collective radiation [23].

V. EXPERIMENTAL PROPOSAL AND TYPICAL PARAMETERS FOR THE MODEL

In this section, we elucidate the experimental feasibility of the proposed atom-cavity system to observe our theoretical predictions. To be specific, one possible platform to implement our present scheme mainly includes an optical cavity, a source of atoms (a pair of neutral atoms), a polarizing beam splitter, and an avalanche photodiode detector.

For the cavity, we make use of optical Fabry-Pérot cavity, involving the two nearly degenerate TEM_{00} modes with orthogonal linear polarizations H and V, which has been successfully realized in Refs. [20,44,52]. Further, it is shown that a slight nondegeneracy (birefringence splitting) of these two orthogonal modes is less than $2\pi \times 0.5$ MHz [20,44]. Here, we set the mode splitting δ_{HV} to be $2\pi \times 0.48$ MHz, satisfying the above requirement. In order to control the length of the cavity, the mirrors are glued directly to flat

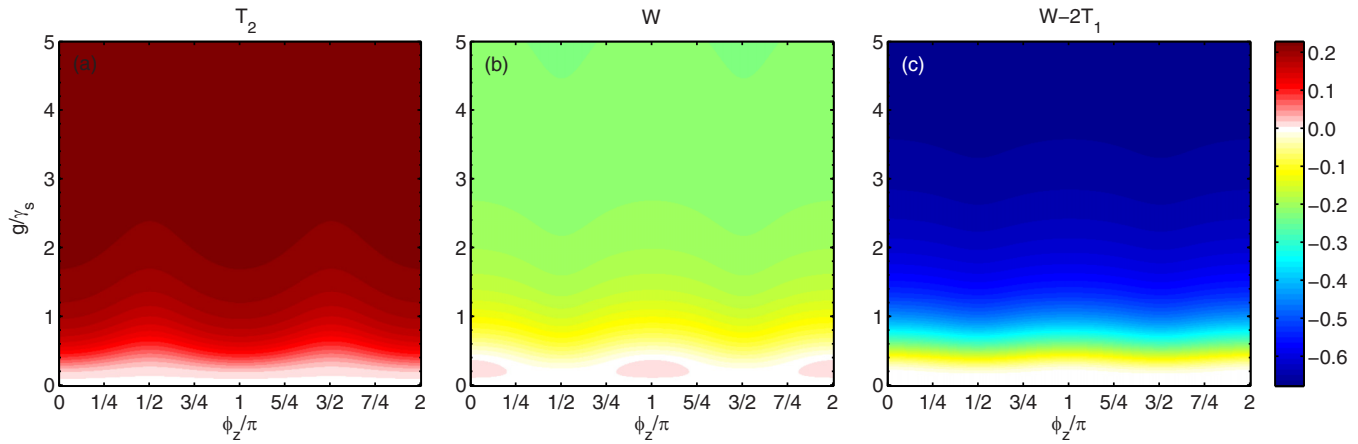

FIG. 7. Contour plots of (a) the normalized intensity transmissions T_2 of the undriven H-polarized cavity mode in the two-atom case, (b) evaluation parameter W of optical-mode-conversion ability, and (c) another evaluation parameter $W - 2T_1$ versus the interatomic-distance-induced phase ϕ_z/π and the atom-cavity coupling strength g/γ_s at $\Delta_V = 0$. The system parameters are $\kappa_{le} = \kappa_{re} = 0.4\gamma_s$, $\kappa_i = 0.03\gamma_s$, $\delta_{HV} = 0.08\gamma_s$, $\delta_{AV} = 0$, $\varphi = \pi/4$, and $\mathcal{E}_p = 0.01\gamma_s$.

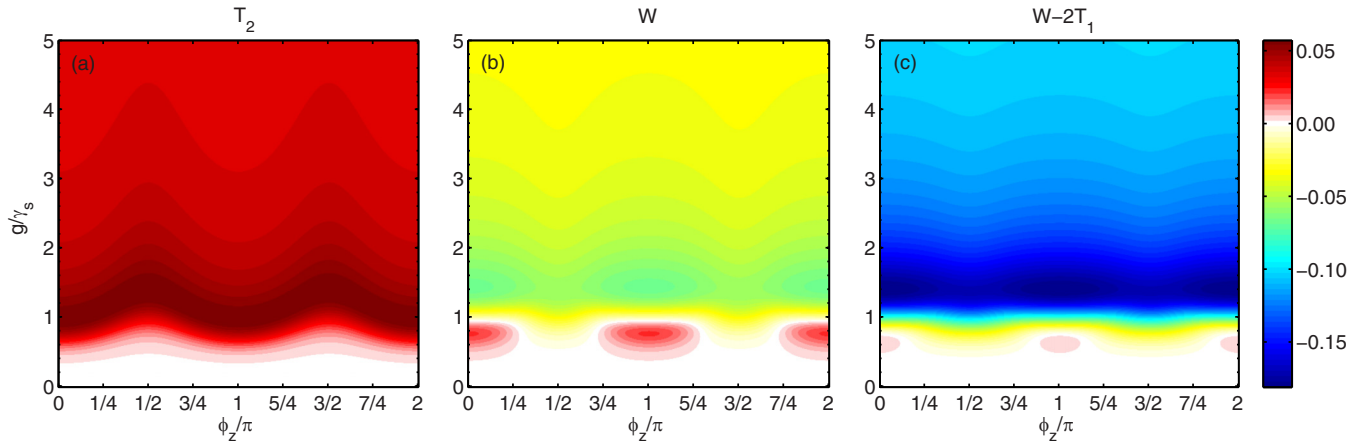

FIG. 8. Contour plots of (a) the normalized intensity transmissions T_2 of the undriven H-polarized cavity mode in the two-atom case, (b) evaluation parameter W of optical-mode-conversion ability, and (c) another evaluation parameter $W - 2T_1$ versus the interatomic-distance-induced phase ϕ_z/π and the atom-cavity coupling strength g/γ_s at $\Delta_V = \gamma_s$. The system parameters are $\kappa_{le} = \kappa_{re} = 0.4\gamma_s$, $\kappa_i = 0.03\gamma_s$, $\delta_{HV} = 0.08\gamma_s$, $\delta_{AV} = 0$, $\varphi = \pi/4$, and $\mathcal{E}_p = 0.01\gamma_s$.

piezoelectric transducers. The cavity length can be stabilized with the Pound-Drever-Hall technique [20,25,44]. For more details about the fabrication procedure of this bimodal cavity in the experiment, see Refs. [20,44,52].

For the source of atoms, we choose the ^{87}Rb atom pair on the $5S$-$5P$ transition (nuclear spin $I = \frac{3}{2}$, D_2 line, and wavelength 780.2 nm [53]) as an example. The other type of qubits like the ions can also be suitable candidates [24,54]. The designated states and the decay rate in the inset of Fig. 1 can be selected as follows: $|1\rangle = |5S_{1/2}, F = 1, m_F = 0\rangle$ and $|2\rangle = |5P_{3/2}, F = 0, m_F = 0\rangle$ together with $\gamma_s = 2\pi \times 6$ MHz [25,53], where F and m_F denote the quantum numbers describing the total atomic angular momentum and its projection onto the quantization axis, respectively. Initially, the two Rb atoms can be captured from background gas by a magneto-optical trap and, subsequently, are loaded into detuned standing-wave optical dipole traps [23]. By means of the combined trapping potential, we can fix one atom at an antinode of the cavity fields (i.e., it is maximally coupled to the cavity), and vary another atom along the cavity axis. Experimentally, via combining an optical lattice for atom localization and an imaging system with single-site resolution, a distance-controlled and deterministically prepared ^{87}Rb atom pair in an optical Fabry-Pérot cavity has been reported; see Refs. [25,55,56] for more details.

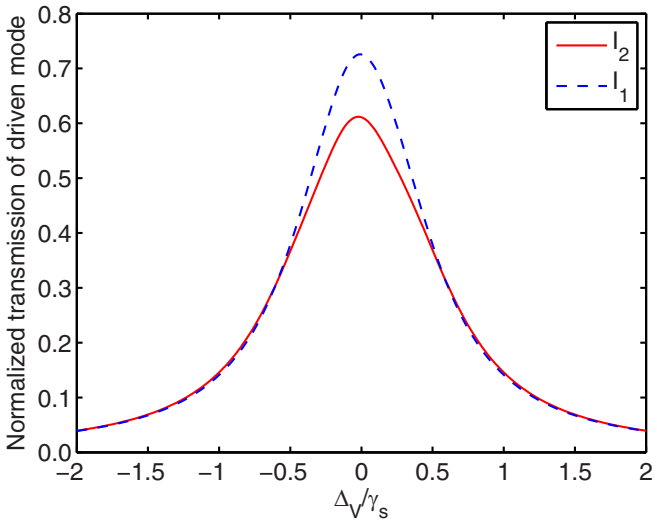

FIG. 9. Normalized intensity transmissions I_2 of the driven V-polarized cavity mode in the two-atom case as a function of the detuning Δ_V/γ_s, and I_1 in the one-atom case. The system parameters are $g = 0.25\gamma_s$, $\kappa_{le} = \kappa_{re} = 0.4\gamma_s$, $\kappa_i = 0.03\gamma_s$, $\delta_{HV} = 0.08\gamma_s$, $\delta_{AV} = 0$, $\phi_z = 0$, $\varphi = \pi/4$, and $\mathcal{E}_p = 0.01\gamma_s$.

In order to separate the two orthogonal linear polarizations, a calcite Wollaston prism (i.e., a polarizing beam splitter) at the cavity output, as indicated in the right side of Fig. 1, is applied. Then, the H-polarized photons along the cavity axis (i.e., the z axis) can be detected by a single-photon avalanche diode.

Finally, we comment on realistic experimental parameters of the system. In our calculations, typical parameters are expressed in units of atomic dipole decay rate γ_s, for ^{87}Rb atoms here, $\gamma_s = 2\pi \times 6$ MHz [53]. We take the cavity with the total loss rate $\kappa = 0.83\gamma_s \simeq 2\pi \times 5$ MHz, where $\kappa_{le} = \kappa_{re} = 0.4\gamma_s = 2\pi \times 2.4$ MHz (symmetric cavity) and $\kappa_i = 0.03\gamma_s = 2\pi \times 0.2$ MHz. For the cavity length of $L = 2.2$ mm [57,58], its finesse is $\mathcal{F} = \pi c/(\kappa L) \simeq 1.4 \times 10^4$ with c being the light speed in free space. We set the atom-cavity coupling strength as $g = 0.25\gamma_s = 2\pi \times 1.5$ MHz [57]. Owing to the fact that $g < (\kappa/2, \gamma_s/2)$ or the cooperativity parameter $C = 4g^2/(\kappa\gamma_s) = 0.3 < 1$, these parameters place our atom-cavity system in the weak-coupling regime of cavity QED (i.e., the bad-cavity regime). The cavity parameter values required above are fairly representative of the generic experimental atom-cavity QED architectures.

VI. CONCLUSIONS AND OUTLOOKS

In summary, we have studied optical-mode-conversion behaviors in a bimodal cavity QED system under the weak excitation of the V-polarized mode, where the H-polarized

light can be well generated by the atomic radiation into the H-polarized mode. Operating in the weak-coupling regime of cavity QED, we present the detailed analytical and numerical results and assess the mode-conversion efficiency from the V polarization to the H polarization. It is revealed that the collective behavior of two atoms in the cavity can effectively enhance optical-mode-conversion efficiency, such as the so-called hyperconversion. We also discuss the experimental feasibility of the scheme by combining currently available technologies of cavity QED and atom traps. In addition to being of fundamental interest, our results may have potential applications in the control over directionality of hyperradiance and hyperconversion, achievable with tunable drive parameters, such as the studies of random lasers [43], as well as the generation of nonclassical fields with hyperradiance and hyperconversion, such as squeezed states and photon antibunching of optical fields [34,36].

Next, although the study that we present is in the context of Fabry-Pérot cavities and the atomic or ionic systems, the results should be applicable to other types of orthogonally polarized two-mode cavities like micropillar cavities [59], H1 photonic crystal cavities [60], and two-level systems like quantum dots and diamond nitrogen-vacancy centers. We thus expect that our findings stimulate new experiments in different domains of physics.

In future work, it will be interesting to explore optical-mode hyperradiance and hyperconversion by extending the bad-cavity limit to the free-space limit. Namely, we remove completely cavity and consider free-space limit. In this free space, although the two cavity modes are absent, we can apply the two free-space lasers (free-space modes [61]) to play the same functionalities as the cavity modes. This will bring more interesting results to the study of strong amplification and correlations in matter-field systems without a dedicated cavity.

ACKNOWLEDGMENTS

We would like to thank the two anonymous referees for many valuable suggestions. We also thank R. Yu for stimulating discussions. This research is supported in part by the National Natural Science Foundation of China (NSFC) through Grant No. 12275092 and by the National Key Research and Development Program of China under Contract No. 2021YFA1400700.

APPENDIX: DERIVATION OF SYSTEM HAMILTONIAN STARTING FROM VECTOR-POTENTIAL REPRESENTATION IN EQ. (1)

As shown in Fig. 1, this coupled cavity-atom system can be described by the total Hamiltonian

$$\hat{H}_{\rm tot} = \hat{H}_{\rm cav} + \hat{H}_{\rm ato} + \hat{H}_{\rm int} + \hat{H}_{\rm dri}. \tag{A1}$$

The four terms of the Hamiltonian are, respectively, the bimodal cavity-field Hamiltonian ($\hat{H}_{\rm cav}$), the two-atom Hamiltonian ($\hat{H}_{\rm ato}$), the atom-field interaction Hamiltonian ($\hat{H}_{\rm int}$), and the external pump driving Hamiltonian ($\hat{H}_{\rm dri}$).

For a bimodal cavity with the V-polarized mode (resonance frequency ω_V) and the H-polarized mode (resonance frequency ω_H), along the lines of Refs. [47,48], the unperturbed Hamiltonian $\hat{H}_{\rm cav}$ takes the second quantization form

$$\hat{H}_{\rm cav} = \sum_{j=H,V} \hbar\omega_j \left(\hat{a}_j^\dagger \hat{a}_j + \frac{1}{2}\right), \tag{A2}$$

where $\hat{a}_j$ and $\hat{a}_j^\dagger$ are photon annihilation and creation operators, respectively. Note that, in the main text and below, we will discard the zero-point energies of $\frac{1}{2}\hbar\omega_j$ $(j = H, V)$ because they only cause an overall energy offset and do not effect the dynamics of the system under consideration.

In order to describe the two-atom Hamiltonian and the interaction Hamiltonian between the atoms and the cavity fields, we need to introduce the electromagnetic vector potential operator $\hat{\mathbf{A}}$ based on a canonical quantization way. Without considering relativistic corrections, such a system involved here is described by the following Hamiltonian:

$$\hat{H}_{cp} = \sum_{i=1,2} \frac{[\hat{\mathbf{p}}_i - q\hat{\mathbf{A}}(\mathbf{r}_i)]^2}{2m} + U(\mathbf{r}_i), \tag{A3}$$

where m and q are the mass and the charge of each electron in the two atoms, whose positions and momenta are depicted by the operators $\hat{\mathbf{r}}_i$ and $\hat{\mathbf{p}}_i$. The first term of the Hamiltonian describes the kinetic energy of the electron in the atoms, while the second term represents the electric potential energy $U(\mathbf{r}_i)$, respectively. Finally, the vector potential at the electron position $\hat{\mathbf{A}}$ can be expressed in the Schrödinger picture as [47,48]

$$\hat{\mathbf{A}}(\mathbf{r}_i) = \sum_{j=H,V} \sqrt{\frac{\hbar}{2\epsilon_0 V\omega_j}} f_j(\mathbf{r}_i)\mathbf{e}_j(\hat{a}_j + \hat{a}_j^\dagger), \tag{A4}$$

where ϵ_0 is the permittivity of vacuum and $\mathbf{e}_j$ is the unit polarization vector of the electric field. $f_j(\mathbf{r})$ indicates the cavity-mode function which depends on the specific geometry of the cavity and can be normalized to be equal to the cavity-mode volume, i.e., $\int d^3r|f_j(\mathbf{r})|^2 = V$. At the same time, $f_j(\mathbf{r})$ should satisfy the Helmholtz equation $\nabla^2 f_j(\mathbf{r}) + \frac{\omega_j^2}{c^2} f_j(\mathbf{r}) = 0$. Worth to note is that this vector potential operator $\hat{\mathbf{A}}(\mathbf{r}_i)$ in Eq. (A4) acts on both the spaces of the two atoms $(i = 1, 2)$ and of the two-mode cavity fields $(j = H, V)$.

When the first term on the right-hand side of Eq. (A3) (i.e., the square in the kinetic energy of the atoms) is expanded, the Hamiltonian $\hat{H}_{cp}$ in Eq. (A3) can be rewritten after some simplifications as

$$\hat{H}_{cp} = \hat{H}_{\rm ato} + \hat{H}_{\rm int} + \hat{H}_{A^2}, \tag{A5}$$

$$\hat{H}_{\rm ato} = \sum_{i=1,2} \frac{\hat{\mathbf{p}}_i^2}{2m} + U(\mathbf{r}_i), \tag{A6}$$

$$\hat{H}_{\rm int} = -\frac{q}{m}\sum_{i=1,2} \hat{\mathbf{p}}_i \cdot \hat{\mathbf{A}}(\mathbf{r}_i) \equiv i\omega_j \sum_{i=1,2} q\hat{\mathbf{r}}_i \cdot \hat{\mathbf{A}}(\mathbf{r}_i), \tag{A7}$$

$$\hat{H}_{A^2} = \frac{q^2}{2m}\sum_{i=1,2} \hat{\mathbf{A}}^2(\mathbf{r}_i), \tag{A8}$$

where we have utilized the relations $\hat{\mathbf{p}} \cdot \hat{\mathbf{A}} = \hat{\mathbf{A}} \cdot \hat{\mathbf{p}}$ due to the Coulomb gauge condition $\nabla \cdot \hat{\mathbf{A}} = 0$ and $\hat{\mathbf{p}} = m\frac{d\hat{\mathbf{r}}}{dt} = -im\omega_j\hat{\mathbf{r}}$ in the derivation process of Eq. (A7). It is worth to mention that the third term $\hat{H}_{A^2}$ [see Eq. (A8)] describes the

two-photon annihilation and creation process in the interaction of the bimodal cavity field with the two atoms. In this work, we neglect this high-order light-matter interaction term.

We consider the two two-level atoms with the lower ground states $|1\rangle_i$ (energy $E_{1i} = E_1$) and the upper excited states $|2\rangle_i$ (energy $E_{2i} = E_2$), and the same transition frequencies $[\omega_A = (E_2 - E_1)/\hbar)]$ between two energy levels of each atom (see the inset of Fig. 1). $|1\rangle_i$ and $|2\rangle_i$ represent a complete basis for each atom. We also assume that the two-level atomic systems with the transition frequency ω_A is on resonance or close to resonance with the cavity-mode frequencies ω_j. According to the quantum-mechanical treatment, the two-atom Hamiltonian $\hat{H}_{\rm ato}$ [see Eq. (A6)] can be recast into

$$\hat{H}_{\rm ato} = \sum_{i=1,2} E_1|1\rangle_i\langle 1| + E_2|2\rangle_i\langle 2| \equiv \sum_{i=1,2} \hbar\omega_A|2\rangle_i\langle 2|. \quad \text{(A9)}$$

In the last step, without loss of generality, we have set the energy of the ground-state level $|1\rangle_i$ as the zero-point energy $E_1 = 0$.

For the dipole interaction term $\hat{H}_{\rm int}$ [see Eq. (A7)] between the atoms and the cavity fields, we make use of the long-wavelength approximation (i.e., the dipole approximation) and assume that the wavelengths λ_j of the two cavity modes are much larger than the atom size a_0 (Bohr radius), i.e., $\lambda_j \gg a_0$. With this approximation, the space dependence of the electromagnetic field can be ignored, therefore, $\hat{\mathbf{A}}(\mathbf{r}_i) \simeq \hat{\mathbf{A}}(\mathbf{r}_{i0})$, with $\mathbf{r}_{i0}$ being the positions of the two atoms inside the cavity. By applying the unity operator (i.e., the complete basis $(|1\rangle_i\langle 1| + |2\rangle_i\langle 2| = 1)$ of two atomic eigenstates $|1\rangle_i$ and $|2\rangle_i$) to both sides of the atomic dipole moment operator $\hat{\mathbf{d}}_i = q\hat{\mathbf{r}}_i$ [see Eq. (A7)] resulting from the separation between the nucleus and electron [62], the dipole interaction Hamiltonian $\hat{H}_{\rm int}$ reads as

$$\hat{H}_{\rm int} = \sum_{i=1,2;j=H,V} \hbar G_{ij}(\hat{\sigma}_i^\dagger + \hat{\sigma}_i)(\hat{a}_j + \hat{a}_j^\dagger), \quad \text{(A10)}$$

where $\hat{\sigma}_i^\dagger$ and $\hat{\sigma}_i$ are the raising and lowering Pauli operators associated with each individual atom with the forms $\hat{\sigma}_i^\dagger = |2\rangle\langle 1|_i$ and $\hat{\sigma}_i = |1\rangle\langle 2|_i$. Above, we have assumed the atomic dipole moment matrix element to be real without loss of generality, where the dipole matrix element $\mathbf{d}_i^{12} = \langle 1|\hat{\mathbf{d}}_i|2\rangle_i$. Finally, we have introduced the coupling parameter between the ith atom and the j-polarized cavity mode, defined as [3,63]

$$G_{ij} = g_{ij}\cos(\varphi_{ij}), \quad \text{(A11)}$$

with

$$g_{ij} = \frac{d_i^{12}}{\hbar}\sqrt{\frac{\hbar\omega_j}{2\epsilon_0 V}} f_j(\mathbf{r}_{i0}), \quad \text{(A12)}$$

$$\cos(\varphi_{ij}) = \frac{\mathbf{d}_i^{12}\cdot\mathbf{e}_j}{d_i^{12}}, \quad \text{(A13)}$$

from which it is clear that the coherent coupling strength between atoms and fields depends on the spatial distribution of the cavity mode $f_j(\mathbf{r}_{i0})$, the relative orientation between the dipole moment of the atom and the polarization of the cavity mode φ_{ij}, and the cavity-mode volume V. Especially, $g_{ij} \propto V^{-1/2}$ reflects that g_{ij} can be increased by decreasing V, i.e., confining the cavity field to a small mode volume.

In the rotating-wave approximation where the terms proportional to $\hat{\sigma}_i\hat{a}_j$ and $\hat{\sigma}_i^\dagger\hat{a}_j^\dagger$ do not conserve energy and can be neglected, the Hamiltonian $\hat{H}_{\rm int}$ in Eq. (A10) can be further simplified and rearranged as

$$\hat{H}_{\rm int} = \hbar g_1[(\hat{a}_V\cos\varphi + \hat{a}_H\sin\varphi)\hat{\sigma}_1^\dagger + \text{H.c.}] + \hbar g_2[(\hat{a}_V\cos\varphi + \hat{a}_H\sin\varphi)\hat{\sigma}_2^\dagger + \text{H.c.}], \quad \text{(A14)}$$

where H.c. denotes the Hermitian conjugate. We have taken $f_j(\mathbf{r}_{i0}) = \cos(2\pi z_i/\lambda_j)$ along the cavity axis z (see Fig. 1) and the transverse mode function $u_j(x_{i0}, y_{i0}) = 1$ for a Fabry-Pérot cavity, $\varphi_{ij} = \varphi$, $d_i^{12} = d^{12}$, and $\omega_j = \omega$, respectively. Under these conditions, g_{ij} is reduced into $g_i = \frac{d^{12}}{\hbar}\sqrt{\frac{\hbar\omega}{2\epsilon_0 V}}\cos(2\pi z_i/\lambda) = g\cos(2\pi z_i/\lambda)$ with $g = \frac{d^{12}}{\hbar}\sqrt{\frac{\hbar\omega}{2\epsilon_0 V}}$ in the main text.

Here, we apply an external pump laser in order to drive the system. The driving term $\hat{H}_{\rm dri}$, which describes the excitation of the V-polarized cavity mode by a coherent pump laser of frequency ω_p, is added in the form

$$\hat{H}_{\rm dri} = \hbar\mathcal{E}_p(e^{-i\omega_p t}\hat{a}^\dagger + e^{i\omega_p t}\hat{a}), \quad \text{(A15)}$$

where $\mathcal{E}_p$ is the driving strength which is proportional to the amplitude of the pump laser. The time dependence of the Hamiltonian $\hat{H}_{\rm dri}$ reflects the nonconservation of the system energy, which is expected because the photons are exchanged with the pump laser.

[1] H. Mabuchi and A. C. Doherty, Cavity quantum electrodynamics: Coherence in context, Science **298**, 1372 (2002).

[2] S. Haroche and J. M. Raimond, *Exploring the Quantum: Atoms, Cavities, and Photons* (Oxford University Press, Oxford, 2006).

[3] J. Vučković, Quantum optics and cavity QED with quantum dots in photonic crystals, in *Quantum Optics and Nanophotonics*, edited by C. Fabre, V. Sandoghdar, N. Treps, and L. F. Cugliandolo (Oxford University Press, Oxford, 2017), pp. 365–406.

[4] H. Walther, B. T. H. Varcoe, B.-G. Englert, and T. Becker, Cavity quantum electrodynamics, Rep. Prog. Phys. **69**, 1325 (2006).

[5] D. Meschede, H. Walther, and G. Müller, One-Atom Maser, Phys. Rev. Lett. **54**, 551 (1985).

[6] K. An, J. J. Childs, R. R. Dasari, and M. S. Feld, Microlaser: A laser with One Atom in an Optical Resonator, Phys. Rev. Lett. **73**, 3375 (1994).

[7] P. W. H. Pinkse, T. Fischer, P. Maunz, and G. Rempe, Trapping an atom with single photons, Nature (London) **404**, 365 (2000).

[8] C. J. Hood, T. W. Lynn, A. C. Doherty, A. S. Parkins, and H. J. Kimble, The atom-cavity microscope: Single atoms bound in orbit by single photons, Science **287**, 1447 (2000).

[9] B. Lounis and M. Orrit, Single-photon sources, Rep. Prog. Phys. **68**, 1129 (2005).

[10] I. Aharonovich, D. Englund, and M. Toth, Solid-state single-photon emitters, Nat. Photonics **10**, 631 (2016).

[11] N. Somaschi, V. Giesz, L. De Santis, J. C. Loredo, M. P. Almeida, G. Hornecker, S. L. Portalupi, T. Grange, C. Anton, J. Demory, C. Gomez, I. Sagnes, N. D. Lanzillotti-Kimura, A. Lemaitre, A. Auffeves, A. G. White, L. Lanco, and P. Senellart, Near-optimal single-photon sources in the solid state, Nat. Photonics **10**, 340 (2016).

[12] A. Reiserer, N. Kalb, G. Rempe, and S. Ritter, A quantum gate between a flying optical photon and a single trapped atom, Nature (London) **508**, 237 (2014).

[13] B. Hacker, S. Welte, G. Rempe, and S. Ritter, A photon-photon quantum gate based on a single atom in an optical resonator, Nature (London) **536**, 193 (2016).

[14] C. H. Bennett and D. P. DiVincenzo, Quantum information and computation, Nature (London) **404**, 247 (2000).

[15] A. Blais, R.-S. Huang, A. Wallraff, S. M. Girvin, and R. J. Schoelkopf, Cavity quantum electrodynamics for superconducting electrical circuits: An architecture for quantum computation, Phys. Rev. A **69**, 062320 (2004).

[16] J. L. O'Brien, A. Furusawa, and J. Vučković, Photonic quantum technologies, Nat. Photonics **3**, 687 (2009).

[17] R. M. Serra, C. J. Villas-Bôas, N. G. de Almeida, and M. H. Y. Moussa, Frequency up- and down-conversions in two-mode cavity quantum electrodynamics, Phys. Rev. A **71**, 045802 (2005).

[18] X. Zou, Y. Dong, and G. Guo, Schemes for realizing frequency up- and down-conversions in two-mode cavity QED, Phys. Rev. A **73**, 025802 (2006).

[19] M. L. Terraciano, R. Olson Knell, D. L. Freimund, L. A. Orozco, J. P. Clemens, and P. R. Rice, Enhanced spontaneous emission into the mode of a cavity QED system, Opt. Lett. **32**, 982 (2007).

[20] J. Straubel, R. Filter, C. Rockstuhl, and K. Słowik, Efficient mode conversion in an optical nanoantenna mediated by quantum emitters, Opt. Lett. **41**, 2294 (2016).

[21] J. Li, R. Yu, J. Ma, and Y. Wu, Proposal for efficient mode converter based on cavity quantum electrodynamics dark mode in a semiconductor quantum dot coupled to a bimodal microcavity, J. Appl. Phys. **116**, 164306 (2014).

[22] S. Yadav, S. Yeasmin, A. B. Bhattacherjee, and S. Banerjee, Far-infrared frequency mode conversion using bulk acoustic phonon modes, Appl. Phys. B **128**, 46 (2022).

[23] R. Reimann, W. Alt, T. Kampschulte, T. Macha, L. Ratschbacher, N. Thau, S. Yoon, and D. Meschede, Cavity-Modified Collective Rayleigh Scattering of Two Atoms, Phys. Rev. Lett. **114**, 023601 (2015).

[24] B. Casabone, K. Friebe, B. Brandstätter, K. Schüppert, R. Blatt, and T. E. Northup, Enhanced Quantum Interface with Collective Ion-Cavity Coupling, Phys. Rev. Lett. **114**, 023602 (2015).

[25] A. Neuzner, M. Körber, O. Morin, S. Ritter, and G. Rempe, Interference and dynamics of light from a distance-controlled atom pair in an optical cavity, Nat. Photonics **10**, 303 (2016).

[26] A. Y. Bazhenov, M. Nikitina, and A. P. Alodjants, High temperature superradiant phase transition in quantum structures with a complex network interface, Opt. Lett. **47**, 3119 (2022).

[27] A. Y. Bazhenov, D. V. Tsarev, and A. P. Alodjants, Mean-field theory of superradiant phase transition in complex networks, Phys. Rev. E **103**, 062309 (2021).

[28] M. Pleinert, J. Von Zanthier, and G. S. Agarwal, Hyperradiance from collective behavior of coherently driven atoms, Optica **4**, 779 (2017).

[29] J. Xu, S. Chang, Y. Yang, S. Zhu, and G. S. Agarwal, Hyperradiance accompanied by nonclassicality, Phys. Rev. A **96**, 013839 (2017).

[30] Q. Bin, X.-Y. Lü, T.-S. Yin, Y. Li, and Y. Wu, Collective radiance effects in the ultrastrong-coupling regime, Phys. Rev. A **99**, 033809 (2019).

[31] J. Han, J. Kim, S.-H. Oh, G. Son, J. Ha, and K. An, Hyperradiance by a stream of phase-correlated atomic dipole pairs traversing a high-Q cavity, Sci. Rep. **11**, 11256 (2021).

[32] L. Droenner, N. L. Naumann, J. Kabuss, and A. Carmele, Collective enhancements in many-emitter phonon lasing, Phys. Rev. A **96**, 043805 (2017).

[33] M.-O. Pleinert, J. von Zanthier, and G. S. Agarwal, Phase control of the quantum statistics of collective emission, Phys. Rev. A **97**, 023831 (2018).

[34] T. Zhao, Y. Yan, G.-q. Yang, G.-m. Huang, Y. Zhu, and G.-x. Li, Multiphoton nonclassical state generated by hyperradiance originating from a quasi-subradiant state, Phys. Rev. A **99**, 043814 (2019).

[35] C. J. Zhu, Y. P. Yang, and G. S. Agarwal, Collective multiphoton blockade in cavity quantum electrodynamics, Phys. Rev. A **95**, 063842 (2017).

[36] J. Li, C. Zhu, and Y. Yang, Squeezed light generated with hyperradiance without nonlinearity, Opt. Lett. **47**, 3439 (2022).

[37] M. O. Scully and M. S. Zubairy, *Quantum Optics* (Cambridge University, Cambridge, England, 1997).

[38] J. I. Cirac, M. Lewenstein, and P. Zoller, Laser cooling a trapped atom in a cavity: Bad-cavity limit, Phys. Rev. A **51**, 1650 (1995).

[39] D. Meiser, J. Ye, D. R. Carlson, and M. J. Holland, Prospects for a Millihertz-Linewidth Laser, Phys. Rev. Lett. **102**, 163601 (2009).

[40] A. Auffèves, D. Gerace, S. Portolan, A. Drezet, and M. F. Santos, Few emitters in a cavity: From cooperative emission to individualization, New J. Phys. **13**, 093020 (2011).

[41] B. Julsgaard and K. Mølmer, Measurement-induced two-qubit entanglement in a bad cavity: Fundamental and practical considerations, Phys. Rev. A **85**, 032327 (2012).

[42] A. Shankar, J. T. Reilly, S. B. Jäger, and M. J. Holland, Subradiant-to-Subradiant Phase Transition in the Bad Cavity Laser, Phys. Rev. Lett. **127**, 073603 (2021).

[43] F. Luan, B. Gu, A. S. L. Gomes, K.-T. Yong, S. Wen, and P. N. Prasad, Lasing in nanocomposite random media, Nano Today **10**, 168 (2015).

[44] D. G. Norris, E. J. Cahoon, and L. A. Orozco, Atom detection in a two-mode optical cavity with intermediate coupling: Autocorrelation studies, Phys. Rev. A **80**, 043830 (2009).

[45] M. Tavis and F. W. Cummings, Exact solution for an *N*-molecule–radiation-field Hamiltonian, Phys. Rev. **170**, 379 (1968).

[46] H. J. Carmichael, *Statistical Methods in Quantum Optics 1*, 2nd ed. (Springer, Berlin, 2002).

[47] G. S. Agarwal, *Quantum Optics* (Cambridge University Press, Cambridge, UK, 2013).

[48] C. W. Gardiner and P. Zoller, *Quantum Noise: A Handbook of Markovian and Non-Markovian Quantum Stochastic Methods*

with Applications to Quantum Optics, 3rd ed., Springer Series in Synergetics (Springer, Berlin, 2004).

[49] A. Reiserer and G. Rempe, Cavity-based quantum networks with single atoms and optical photons, Rev. Mod. Phys. **87**, 1379 (2015).

[50] E. Mascarenhas, D. Gerace, M. F. Santos, and A. Auffèves, Cooperativity of a few quantum emitters in a single-mode cavity, Phys. Rev. A **88**, 063825 (2013).

[51] R. H. Dicke, Coherence in spontaneous radiation processes, Phys. Rev. **93**, 99 (1954).

[52] T. D. Barrett, O. Barter, D. Stuart, B. Yuen, and A. Kuhn, Polarization Oscillations in Birefringent Emitter-Cavity Systems, Phys. Rev. Lett. **122**, 083602 (2019).

[53] D. A. Steck, "Rubidium 87 D Line Data," available online at http://steck.us/alkalidata (revision 2.2.2, 9 July 2021).

[54] B. Casabone, A. Stute, K. Friebe, B. Brandstätter, K. Schüppert, R. Blatt, and T. E. Northup, Heralded Entanglement of Two Ions in an Optical Cavity, Phys. Rev. Lett. **111**, 100505 (2013).

[55] S. Welte, B. Hacker, S. Daiss, S. Ritter, and G. Rempe, Cavity Carving of Atomic Bell States, Phys. Rev. Lett. **118**, 210503 (2017).

[56] S. Welte, B. Hacker, S. Daiss, S. Ritter, and G. Rempe, Photon-Mediated Quantum Gate between Two Neutral Atoms in an Optical Cavity, Phys. Rev. X **8**, 011018 (2018).

[57] M. L. Terraciano, R. Olson Knell, D. G. Norris, J. Jing, A. Fernandez, and L. A. Orozco, Photon burst detection of single atoms in an optical cavity, Nat. Phys. **5**, 480 (2009).

[58] K. Kustura, C. Gonzalez-Ballestero, A. de los Ríos Sommer, N. Meyer, R. Quidant, and O. Romero-Isart, Mechanical Squeezing via Unstable Dynamics in a Microcavity, Phys. Rev. Lett. **128**, 143601 (2022).

[59] H. J. Snijders, J. A. Frey, J. Norman, H. Flayac, V. Savona, A. C. Gossard, J. E. Bowers, M. P. van Exter, D. Bouwmeester, and W. Löffler, Observation of the Unconventional Photon Blockade, Phys. Rev. Lett. **121**, 043601 (2018).

[60] Y. Ota, M. Shirane, M. Nomura, N. Kumagai, S. Ishida, S. Iwamoto, S. Yorozu, and Y. Arakawa, Vacuum Rabi splitting with a single quantum dot embedded in a H1 photonic crystal nanocavity, Appl. Phys. Lett. **94**, 033102 (2009).

[61] K. M. Beck, W. Chen, Q. Lin, M. Gullans, M. D. Lukin, and V. Vuletić, Cross Modulation of Two Laser Beams at the Individual-Photon Level, Phys. Rev. Lett. **113**, 113603 (2014).

[62] H. Friedrich, *Theoretical Atomic Physics* (Springer, Berlin, 2006).

[63] P. R. Berman, *Cavity Quantum Electrodynamics* (Academic, Boston, 1994).